Eur. Phys. J. B **14**, 191–200 (2000)

THE EUROPEAN PHYSICAL JOURNAL B

EDP Sciences

Laser Doppler velocimetry analysis of transitional pipe flow

E. Nino[1] and C. Serio[2,a]

[1] Dipartimento di Ingegneria e Fisica dell'Ambiente, Univerista della Basilicata, 85100 Potenza, Italy
[2] Istituto Nazionale di Fisica della Materia, Genova, Italy

Received 29 March 1999 and Received in final form 6 September 1999

Abstract. The objective of this study has been to experimentally analyze the correlation structure of the strong temporal intermittency which characterizes pipe flow close to the transition to turbulence. In doing so transitional pipe flow has been analyzed by Laser Doppler velocimetry and the Reynolds number dependence of the covariance function has been studied. The range which has been analyzed covers the transition to turbulence and moderately developed turbulence (Reynolds number from 1 500 to 5 000). The correlation structure which has been evidenced is generally in agreement with the deterministic, dynamical, interpretation of temporal intermittency which explains the intermittent behavior as a result of a saddle node bifurcation. However, the analysis has evidenced fluctuations even before the onset of turbulence. The structure of these fluctuations is perfectly autoregressive which leads us to conclude that the transition to turbulence can be viewed as a transition from linear randomness to (non-linear) homogeneity.

PACS. 05.40.-a Fluctuation phenomena, random processes, noise, and Brownian motion – 47.20.-k Hydrodynamic stability – 47.27.-i Turbulent flows, convection, and heat transfer

1 Introduction

Transition to turbulence in pipe flow is still now an important fundamental problem in fluid mechanics (*e.g.* [1,2] and references therein). From a mathematical point of view, pipe flow is believed to be linearly stable and yet it is observed to be unstable in the laboratory. According to Wygnanski and Champagne [3,4] unstable flow results from instabilities in the inlet region of the pipe where turbulent patches may be generated by sharp entry geometries and/or instability in the boundary layer. Above a critical value of the Reynolds number (Re) these turbulent patches do not decay when they move along the tube so that, at a fixed point in the pipe, turbulent and laminar motion may be alternatively observed. This phenomenon yields a strong temporal intermittency which has been recognized as one of the fundamental mechanism for the transition to turbulence [5–9]. Laser Doppler velocimetry (LDV) analysis of the correlation structure of this kind of intermittency has been the main objective of this experimental study. In doing so the Reynolds number dependence of the covariance function has been studied. The range we have analyzed covers the transition to turbulence and moderately developed turbulence (Reynolds number from 1 500 to 5 000). The flow configuration which has been analyzed is that obtained in a pipe with a constant pressure head. Turbulent patches were induced by a sharp inlet. The attention is then focused on the structure of the turbulent patches and their propagation along the tube.

From a theoretical point of view, the onset of turbulence through temporal intermittency has been extensively studied by Manneville and Pomeau [9]. Dynamical systems which exhibit temporal intermittency are characterized by a regular motion in phase space, interrupted by randomly distributed bursts of strong chaoticity. According to Manneville and Pomeau [9], the frequency of turbulent bursts increases as the Reynolds number rises above a critical value, $\mathrm{Re_c}$ (for our experiment this critical Re falls in the interval 1 800-2 100). More precisely the time duration of laminar phases is proportional to some power of $1/(\mathrm{Re} - \mathrm{Re_c})$ so that for Re which approaches the critical value, the laminar period diverges and there is no temporal intermittency. Conversely, when Re becomes large, the period of the laminar phases becomes zero and the flow becomes homogeneously turbulent.

According to Manneville and Pomeau [9], three types of intermittency may be distinguished which correspond to a saddle-node or tangent bifurcation (Type I), Hopf bifurcation (Type II) and period-doubling (Type III), respectively. However, the intermittency we have observed is consistent with a tangent or saddle-node bifurcation (Type I) in which a stable fixed point degenerates in a chaotic attractor. Although, stochasticity still plays an important role. According to our findings the flow is characterized by an autoregressive stochastic behavior rather than by a pure linear deterministic dynamics, even before the transition to turbulence, therefore the phenomenon

[a] e-mail: serio@unibas.it

would be better described in the framework of noisy rather than deterministic maps. This may have important implications on the modeling of natural open systems since it stresses the importance of an endogenous noise component evolving with the basic set of governing equations. Nevertheless, it has to be stressed that the non-linearity, as correctly suggested, *e.g.* by Ruelle [8], has a leading role in the transition. The presence of intermittent bursts cannot be explained as an increase in the level of the linear fluctuations. It will be shown, indeed, that these bursts have the same correlation structure as the one which characterizes the developed turbulence, *i.e.* non-autoregressive.

The paper is organized as follows. After presenting the experimental details along with some basic numerical aspects of our analysis (Sect. 2), the mechanics of the intermittent transition is briefly discussed (Sect. 3). Section 4 mainly focuses on the correlation structure of the flow for different values of the Reynolds number. Conclusions are drawn in Section 5.

2 Experimental apparatus

Our measurements have been made in a water tunnel (Fig. 1). Basically, the hydraulic part is a closed water tunnel comprised of an horizontal cylindrical pipe 6 m long, whose inner and outer diameters are 0.05 and 0.06 m, respectively, and a water tank which provides water to the horizontal pipe by a direct coupling through a smooth plastic tube whose diameter is 1/5 of the diameter of the water tunnel. This kind of coupling realizes a sort of sudden expansion (aspect ratio 5:1) which produces a large disturbance at the inlet so that we expect the development of weakly turbulent flow also at very modest values of the Reynolds number. Note that unlike it might appear from the schematic diagram of Figure 1, the entry geometry does not involve sharp edges or corners and there are not regions of separated flow. The discharge from the tunnel is obtained through a sudden contraction which reduces the diameter from 5 cm to 1 cm; the outlet has, therefore, a geometry which parallels that at the inlet.

An adjustable hydraulic level (see Fig. 1) allows us to obtain different flow regimes. A secondary hydraulic circuit powered by two pumps provides to send back the water to the tank. The secondary circuit has been specifically realized in such a way to maintain a constant hydrostatic pressure drop between the tank and the inlet side of the water tunnel.

The turbulence we observe is the result (i): of disturbances at the inlet and (ii) instability of the boundary layer in the inlet region of the pipe. Because of the relatively small value of the Reynolds number we have examined, we expect the first kind of turbulence to dominate.

The LDV system is comprised of an optical part and a data acquisition system. The optical part was developed at our laboratory. The test volume is obtained by two incident laser beams generated by a single 10 mW He-Ne Laser. To avoid undesirable refraction from the pipe wall a rectangular cell filled with water was placed around the pipe at the point where measurements were taken. The two beams are obtained by a rotating diffraction grating. The speed of rotation can be varied in order to produce a frequency shift between the two crossing beams, which, in turn, allows us to be sensitive to the sign of the velocity. The diffraction grating is driven by a tunable digitally controlled brushless-motor. For the experiment described in this paper, the shift allowed between the two beams was 0.1 MHz. This value is optimized for the low velocity range which has been examined in this study.

The data acquisition system is a TSI digital burst correlator, model IFA-655, which has been used with the following operating parameters:

- minimum number of cycles per burst: 8 (this is the maximum allowed by the system);
- signal-to-noise-ratio mode: high;
- threshold optimization: 55%;
- acquisition mode: Random;
- data sampling method: TBD on.

This last operation mode means that the system was operated in such a way to count up the particles passing through the test volume, so that, in addition to velocity observations, the time between samples was recorded, too. In this way almost continuous time records were obtained and proper weight could be given to each sample so that mean velocities and higher order moments could be calculated with little or no bias caused by the particle arrival statistics. No artificial seeding was employed. The sampling rate depended on the Reynolds number. However, it was never less than 100 Hz.

The nearly continuous series was, then, digitally low pass filtered (re-sampled) in order to have equi-spaced samples. The re-sampling rate is given by $\Delta t = r_o \bar{V}^{-1}$, where r_o, has been set equal to the linear dimension of the LDV test space which, in turn, determines the smallest resolvable scale by our equipment, $r_o = 1$ mm. Furthermore, $\bar{V}$ is the mean value of the velocity time series. The low-pass filtering operation consists simply in computing the average value of the velocity during the time interval Δt,

$$V(i\Delta t) = \frac{1}{\Delta t} \sum_{j=1}^{n_i} \Delta t_{ij} u_{ij}; \quad \sum_{j=1}^{n_i} \Delta t_{ij} = \Delta t; \quad i = 1, \ldots, \frac{T}{\Delta t} \tag{1}$$

where u_{ij} indicates the original velocity time series, Δt_{ij} is the time between two consecutive samples $u_{i,j}$, $u_{i,j+1}$; T is the total observational period and, finally, n_i gives the number of velocity samples within each time interval Δt.

The sampling interval, Δt, average value, standard deviation and other parameters relevant to the velocity time series analyzed in this paper are summarized in Table 1. The number of data points which is shown in Table 1 is that obtained after the re-sampling procedure outlined above. The number of data points, before the resampling operation and for the four Reynolds numbers here considered, is 20×10^6 for Re = 1 500, and for Re = 5 000, 6×10^6 for Re = 2 000 and 12×10^6 for Re = 2 500, respectively.

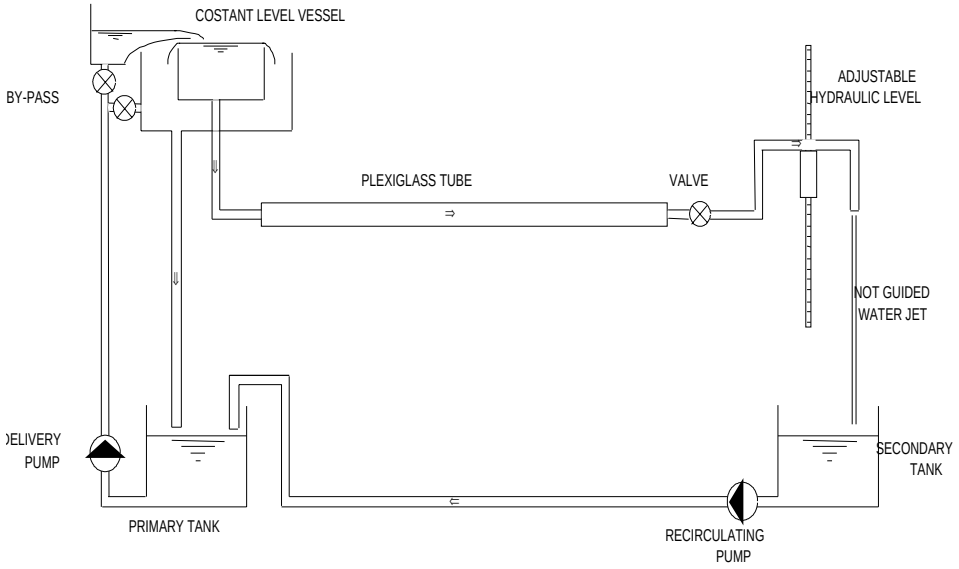

Fig. 1. Schematic setup of the water tunnel. The plexiglas pipe is 6 meters long. The inner and outer diameter of the pipe are 0.05 and 0.06 meters, respectively.

Table 1. Mean ($\bar{V}$), variance ($C(0)$) and number of data points (N) for each time series analyzed in this paper. The table also shows the sampling time Δt, the measurement or LDV noise $\sigma_{\rm w}^2$ and the effective turbulence ratio computed according to $\mathrm{Tu} = \sqrt{C(0) - \sigma_{\rm w}^2}/\bar{V}$. The digits shown for the different quantities are not affected by measurements error.

Reynolds Number	$\bar{V}$ (ms^{-1})	$C(0)$ (m^{2}s^{-2})	N	Δt (s)	$\sigma_{\rm w}^2$ (m^{2}s^{-2})	Tu (%)
Re = 1 500						
$X/d = 20$	0.04999	3.20×10^{-6}	2 022 759	0.020	3.88×10^{-7}	3.3
$X/d = 60$	0.05477	1.60×10^{-6}	2 178 856	0.018	5.50×10^{-7}	1.9
$X/d = 100$	0.05886	1.19×10^{-6}	2 135 316	0.017	9.13×10^{-7}	0.9
Re = 2 000						
$X/d = 100$	0.07505	9.55×10^{-6}	831 227	0.013	1.37×10^{-6}	3.8
Re = 2 500						
$X/d = 100$	0.07150	3.84×10^{-6}	1 840 492	0.014	8.39×10^{-7}	8.6
Re = 5 000						
$X/d = 20$	0.12477	2.70×10^{-5}	3 235 882	0.0080	2.31×10^{-6}	4.0
$X/d = 60$	0.12549	3.11×10^{-5}	3 354 559	0.0079	2.38×10^{-6}	4.3
$X/d = 100$	0.12796	3.21×10^{-5}	3 229 227	0.0078	2.33×10^{-6}	4.3

The Reynolds number is defined as usual:

$$\mathrm{Re} = \frac{Ud}{\nu} \tag{2}$$

with U the mean flow velocity and $\nu = 10^{-6}$ m^{2}s^{-1} the kinematic viscosity of water at 20 °C.

Because of experimental restrictions, only the component of the velocity in the stream wise direction has been measured. Measurements were considered at three different positions along the tube: $X/d = 20, 60, 100$, where X gives the distance from the inlet and d is the inner diameter of the tube.

2.1 Assessing the magnitude of LDV noise

Especially at low flow velocity, the analysis of the correlation structure on the basis of variance spectra is hampered by the inherent LDV noise component (the so-called ambiguity spectrum, [10]) which adds a constant to the observed spectrum and tends to level-off the spectrum of the signal. The effect of this constant white noise component can be seen, *e.g.*, in Figure 2 which shows the variance spectrum for Re = 5 000. It puts a limit to the highest turbulence frequency which can be observed.

Nevertheless, this kind of noise is Gaussian, white and has a constant variance [10]. It affects additively the signal so that the observations can be represented according to

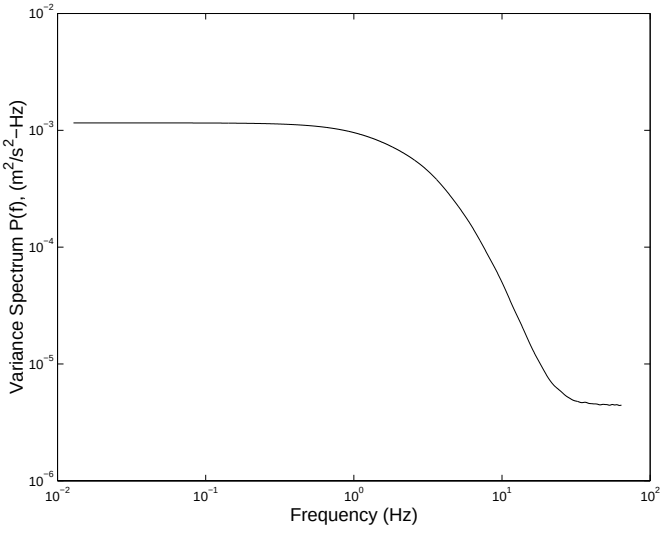

Fig. 2. Variance spectrum of the velocity fluctuations for Re = 5 000.

the following measure model:

$$V(n\Delta t) = V_{\rm s}(n\Delta t) + w(n\Delta t); \quad n = 1, \ldots, N \tag{3}$$

with N the number of data points and Δt the sampling interval. For the sake of simplicity, in the following we will assume $\Delta t = 1$ and we will write $x(n\Delta t) = x(n)$ where x is a generic variable. In equation (3), $V(n)$ is the observed velocity, $V_{\rm s}(n)$ is the *true* velocity signal and $w(n)$ is a white component, uncorrelated and with zero mean and variance $\sigma_{\rm w}^2$.

Because of (3) the observed spectrum $P(f)$ is:

$$P(f) = P_{\rm s}(f) + 2\sigma_{\rm w}^2 \tag{4}$$

where $P_{\rm s}(f)$ denotes the signal spectrum with f the ordinary frequency limited to the normalized Nyquist interval 0-0.5. From equation (4) it is evident that the noise variance, $\sigma_{\rm w}^2$ may be estimated directly by the observed spectrum $P(f)$. To this end it suffices to fit a straight line to the flat portion of the spectrum at higher frequency.

Using this procedure we have estimated the noise variance for the time series at hand, and the results can be read in Table 1. Once an estimate of $\sigma_{\rm w}^2$ has been obtained, the effective turbulence ratio, Tu, may be computed as $\mathrm{Tu} = \sqrt{\sigma^2 - \sigma_{\rm w}^2}/\bar{V}$. Here, σ^2 is the variance of the data points.

Equation (4) says that the white noise affects the spectrum at all frequencies. However, if we consider the covariance function, then, denoting with $C(\tau)$ the observed covariance at the normalized time-lag τ and with $C_{\rm s}$ the covariance function of the signal,

$$C(\tau) = \begin{cases} \sigma_{\rm s}^2 + \sigma_{\rm w}^2 & \text{for } \tau = 0 \\ C_{\rm s}(\tau) & \text{otherwise} \end{cases} \tag{5}$$

provided that the noise component $w(n)$ is white. In equation (5), $\sigma_{\rm s}^2$ is the variance of the signal and $\sigma_{\rm w}^2$ is the variance of the error term, and $\sigma^2 = \sigma_{\rm s}^2 + \sigma_{\rm w}^2$ is the variance of the observations. Equation (5) shows that in presence of a white additive error component, the covariance function is biased only at the origin. This effect may be easily removed by subtracting a suitable estimate of $\sigma_{\rm w}^2$ computed, *e.g.*, as indicated above.

Relation (5) holds for *true* quantities. In practice, the covariance function has to be estimated on the basis of a limited record of data points:

$$C(\tau) = \frac{1}{N}\sum_{j=1}^{N-\tau}(V(j+\tau) - \bar{V})(V(j) - \bar{V}) \tag{6}$$

with $\bar{V}$ the mean value of the series $V(n)$. At any lag τ, $C(\tau)$ will be the composition of signal and noise covariance

$$C(\tau) = C_{\rm s}(\tau) + C_{\rm w}(\tau) \tag{7}$$

with the index s and w denoting signal and noise, respectively. However, for $\tau \neq 0$, we have [11]:

$$\begin{cases} E(C_{\rm w}(\tau)) & = 0 \\ \mathrm{var}(C_{\rm w}(\tau) & = \frac{\sigma_{\rm w}^4}{N} \end{cases} \tag{8}$$

where E indicates expectation and var stands for variance. The second of relation (8) says that the effect of the noise tends to zero as N becomes large. We stress that in our case N is larger than 10^6, which means in practice than the noise, has no relevant effect over the non-null values of the covariance function of the observations and in any case relation (8) provides the correct mean square error for the covariance estimated through relation (6).

In conclusion, the small scale of motion are better observed by considering the covariance function, since this function is fairly insensitive to the noise in the limit in which N becomes large.

3 The intermittent transition

Figure 3 shows segments of the velocity time series for the four Reynolds numbers considered in our analysis. The data shown in Figure 3 were recorded 100 diameters downstream ($X/d = 100$).

The transitional, intermittent, character of the flow is quite evident. For Re = 1 500 we saw a rather erratic behavior around a mean value. However, for Re = 2 000, the presence of intermittent bursts was striking. The frequency of these bursts greatly increase for Re = 2 500. The strong temporal intermittency was no longer visible for Re = 5 000.

The phenomenology and the mechanism of temporal intermittency is quite well understood [3]. It is due to the formation of turbulent patches in the inlet region of the tube. Below a critical value, $\mathrm{Re_c}$, of the Reynolds number (which for our experiment falls in the interval 1800-2100), the turbulence generated in the inlet region tends to decay when the flow progresses along the tube. Above $\mathrm{Re_c}$, some of the turbulent patches do not decay so that we

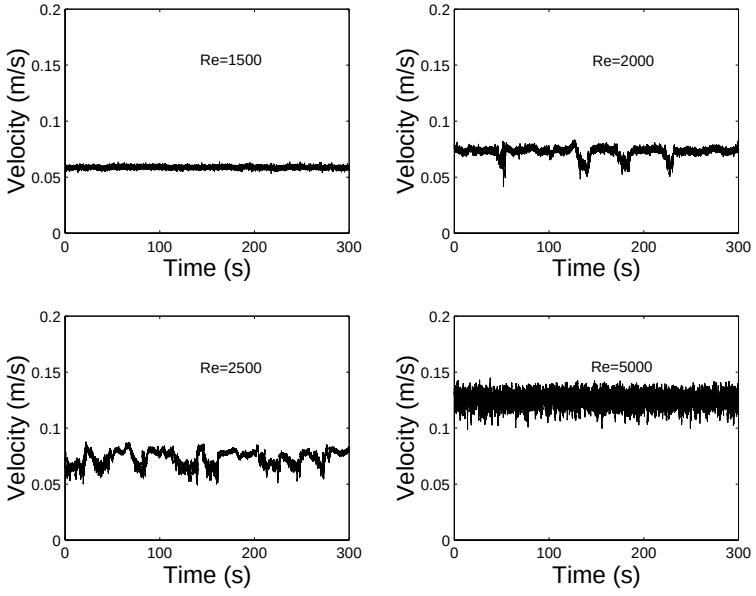

Fig. 3. Velocity time history for $X/d = 100$ and for the Reynolds numbers: Re = 1 500, Re = 2 000, Re = 2 500, Re = 5 000, respectively.

may observe, alternatively, decaying turbulence or growing patches, hence the phenomenon of temporal intermittency. For Re greater than $\mathrm{Re_c}$, the patches grow and spread rapidly through the tube so that the turbulence fills all the pipe. At this stage (Re $\geq$ 4 000) we have developed turbulence.

This behavior is qualitatively in agreement with the intermittent route to turbulence predicted by Manneville and Pomeau [9]. In analogy with a second-order phase transition, these authors postulate the presence of a critical value for the Reynolds number, $\mathrm{Re_c}$, and assume that the laminar phases last a typical characteristic time, $\mathcal{T}$ which satisfies the power-law relation:

$$\mathcal{T} \sim (\mathrm{Re} - \mathrm{Re_c})^{-\gamma} \quad \mathrm{Re} > \mathrm{Re_c} \text{ and } \gamma > 0. \tag{9}$$

Then, for Re which approaches the critical value, the time duration of laminar phases becomes infinity, whereas for $\mathrm{Re} \gg \mathrm{Re_c}$ the period tends to zero and we have only the turbulent phase.

The qualitative agreement between this scenario and our results is evident from the sequence of events shown in Figure 3. For Re = 1 500 we have no evidence of bursts, from which we could argue that the laminar phase lasts infinity. From Re = 2 000 to 2 500 the frequency of bursts clearly increases with Re, hence the duration of the laminar phases decreases with Re. Finally, for Re = 5 000, we have no evident presence of laminar insertions, so that we could argue that now the duration of the laminar phases is zero. A quantitative analysis of the duration of laminar phases has been accomplished out by various author (*e.g.* see [12,13]. In particular, Zhang *et al.* [13] found that the intermittent factor γ is close to 1. Furthermore, these authors showed that stochastic arguments accounted well for their experiment. Although, with a different methodology and experimental apparatus, our findings agree with those of Zhang *et al.* [13] and indicates that the leading mechanism is the random generation of turbulent patches at the pipe entrance, along with energy dissipation due to fluid viscosity and friction. Our methodology directly addresses the nature of velocity fluctuations as will be shown in the next section.

4 Statistical characterization of the transition

An ergodic dynamical system evolving on an attracting set may be represented through the evolution equation of one of its variables [14]. For systems sampled at discrete time, the description is obtained through a finite-difference equation:

$$x(n) = F(x(n-1), x(n-2), ..., x(n-m)) \tag{10}$$

where F is a smooth, generally unknown function, $x(n)$ denotes a generic variable of the system at the discrete-time $n\Delta t$. The auto-regression over m previous realizations of the variable gives the needed initial conditions. Traditionally chaos has referred only to a purely deterministic system and has been considered a distinct alternative to stochastic modeling. However, from a physical point of view, for systems which have attained their stationary state, it is much more interesting to understand whether F is linear or not without the presupposition that the system is deterministic. The description of dynamical systems may be then generalized to include stochasticity simply by adding on the right hand side of equation (10) an additive noisy term [15]:

$$x(n) = F(x(n-1), x(n-1), ..., x(n-m)) + w(n) \tag{11}$$

where the noisy term is added to the evolution equation, and therefore it evolves with the map (endogenous noise).

If F is linear then the above equation defines an autoregressive process [11]. Although equation (11) is a stochastic process, its covariance function is strictly deterministic.

If F is linear, the covariance function is given by the following relation:

$$C_{\rm s}(\tau) = C_{\rm s}(0) \sum_{i=1}^{p} a_i \cos(2\pi \frac{\tau}{T_i}) \exp(-\frac{\tau}{\tau_i}) \qquad (12)$$

with the normalizing condition

$$\sum_{i=1}^{p} a_i = 1 \qquad (13)$$

where p is the number of oscillating modes of the system and the parameters T_i and τ_i depends on the given system. Relation (12) holds provided that the system is stationary. When $m = 1$ then the only possibility is $p = 1$ and only an exponential damping is possible. For $m = 2$ it is possible to have an oscillating mode or a combination of two exponential decays. If F is not linear then the covariance function will be no more represented by relation (12). Thus, the discrimination between an autoregressive (linear) process (which gives place to regular attractors) and a non-linear one (non-regular attractor) may be simply based on testing whether or not relation (12) provides a good model for the correlation structure of the series at hand.

It may happen that even for a non-linear F, the system may attain a regular attractor. However, in this case the correlation structure has still to obey relation (12). In other words, our method looks at the correlation properties rather than directly at the shape of F and therefore cannot be fooled by trivial non-linearity.

This methodology may be infinitely sophisticated and it provides, indeed, the common background to the short-term predictability methods to identify chaos which dates back to Farmer and Sidorowich [16]. The formalization of the method in the context of auto-regressive processes has been provided by one of the authors [17,18]. Since, for this experiment the covariance function may be computed with high accuracy, there is no need to introduce extra-complications.

According to the above methodology, our analysis will be mostly based on the covariance function (de-biased at the origin for the effect of LDV noise; see Sect. 2.1) of the velocity fluctuations.

We will begin with the analysis of the disturbances which originate close to the inlet region. These disturbances may be viewed as the *driving* force of the velocity fluctuations far away from the inlet. As shown in the previous section, it is just the way in which these disturbances progress along the pipe which originates the temporal intermittency.

4.1 The inlet turbulence, X/d = 20

Close to the inlet, the covariance function, irrespective of the Reynolds number, is well reproduced by a pure algebraic model (*e.g.*, see Fig. 4 which illustrates the case Re = 1 500)

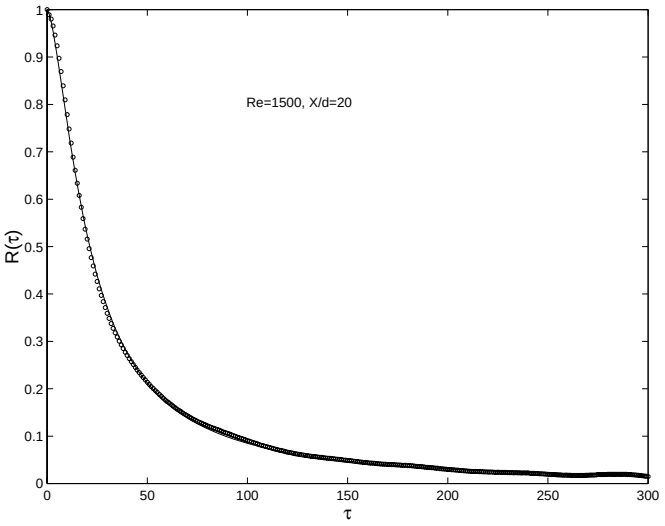

Fig. 4. Covariance function (circles) normalized to the variance of the series, $R(\tau) = C_{\rm s}(\tau)/C_{\rm s}(0)$, against the normalized time scale, τ. The Reynolds number is 1 500, $X/d = 20$. The solid line is the model fitted to the data points.

$$R(\tau) = \frac{C_{\rm s}(\tau)}{C_{\rm s}(0)} = \frac{a}{a + \tau^{\alpha}} \qquad (14)$$

where $C_{\rm s}(0)$ is the variance of the signal, a and α are parameters to be determined.

The model (14) can be also put in the form

$$\frac{C_{\rm s}(\tau)}{C_{\rm s}(0)} = \frac{1}{1 + (\frac{\tau}{\tau_{\rm o})^{\alpha}}} \qquad (15)$$

with $\tau_{\rm o} = a^{(1/\alpha)}$.

According to our results, the exponent α is fairly independent of Re, whereas the cut-off scale critically depends on Re, the higher Re, the smaller $\tau_{\rm o}$, as it is to be expected, since this scale is simply associated to the average size of the disturbances, that is the turbulent patches, generated at the inlet. While the shape of the disturbances which is determined by the exponent α does not change (the mechanism which generates the turbulence remains the same), their size tends to decrease as Re increases because the flow becomes much more turbulent.

The best fit values for $\tau_{\rm o}$ and α are $\tau_{\rm o} = 21.80 \pm 0.09$, $\alpha = 1.636 \pm 0.004$, in the case of Re = 1 500. For Re = 5 000, we have $\tau_{\rm o} = 8.30 \pm 0.05$, $\alpha = 1.619 \pm 0.006$.

It should be noted that the covariance function of the observations tends to zero as τ becomes large which leads us to conclude that the underlying process is stationary. Furthermore, the covariance function is badly reproduced by a linear autoregressive model, which means that in a phase space description the system does not evolve on a regular attractor.

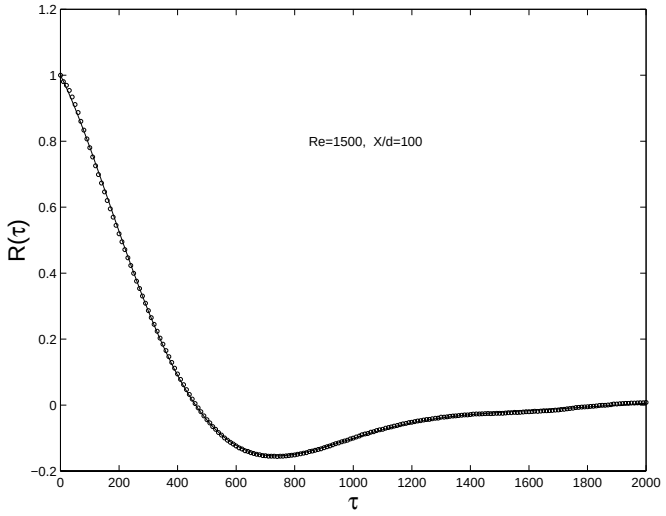

Fig. 5. Covariance function (circles) normalized to the variance of the series, $R(\tau) = C_s(\tau)/C_s(0)$, against the normalized time scale, τ. The Reynolds number is 1 500, $X/d = 100$. The solid line is the model fitted to the data points.

4.2 Turbulence far away from the inlet

In this section, we will focus on the correlation structure of the flow far away from the inlet. For the sake of brevity, we will mostly limit ourselves to consider the case $X/d = 100$. At this distance from the inlet the intermittent transition is fairly well-observed.

We will start with the correlation structure before the intermittent transition (Re = 1 500), then we will be dealing with the case after the transition (*i.e.* Re = 5 000). The transitional region will be described in the end, since this case encompasses aspects which are peculiar to both laminar and turbulent flow.

4.2.1 Re = 1 500, X/d = 100

Below a critical Re, which for our experiment falls in the interval 1800-2100, the turbulence generated at the inlet just decays while the flow moves downstream. This can be seen for Re = 1 500. From Table 1, we have that for $X/d = 20$ the turbulence intensity is about 3%, the intensity becomes less than 2% at a distance of 60 diameters downstream and is less than 1% at 100 diameters downstream.

The observed covariance function for $X/d = 100$ is shown in Figure 5. Comparing this figure to Figure 4, which shows $R(\tau)$ for $X/d = 20$, the dramatic change in the correlation structure emerges evident. The covariance function becomes negative, which indicates the presence of an oscillatory component, although dampened, in the velocity time series.

For this case the observed covariance function is well fitted by a linear process (model (12) with $p = 2$). The comparison between model and observations is provided in Figure 5. The best fit values for the six parameters: a_1 and a_2, T_1 and T_2, τ_1 and τ_2 are here summarized:

$$\begin{cases} a_1 = 0.574 \pm 0.006 & a_2 = 1 - a_1 = 0.426 \pm 0.006 \\ T_1 = 2385 \pm 6 & T_2 = 1328 \pm 3 \\ \tau_1 = 626 \pm 3 & \tau_2 = 493 \pm 2. \end{cases} \quad (16)$$

Relation (12) is the covariance function of a stochastic autoregressive (linear) process. The Fourier transform of this covariance function gives the power spectrum, $P(f)$,

$$\frac{P_s(f)}{C_s(0)} = \sum_{i=1}^{2} \frac{2a_i\gamma_i}{\gamma_i^2 + [2\pi f - \beta_i]^2} + \sum_{i=1}^{2} \frac{2a_i\gamma_i}{\gamma_i^2 + [2\pi f + \beta_i]^2} \quad (17)$$

where f is the usual frequency and $\gamma_i = 1/\tau_i$, $\beta_i = 2\pi/T_i$. For f which becomes large, we have:

$$P_s(f) \sim f^{-2}. \quad (18)$$

This last result is completely analogous to the basic law of Brownian motion and illustrates how systems which mimic Brownian motion may simple arise as limiting case of mere autoregressive (linear) stationary processes.

It should be stressed that the various time constants appearing in the formula above for the covariance function are not strictly related with the size of the disturbances at the inlet, when rather with the way these disturbances decay along the tube. The decay is related to the geometry of the whole tube, fluid viscosity and the friction that the patches experiences while moving downstream. The correlation structure of the disturbances has been shown to be algebraic-like (see Sect. 4.1), whereas the form of the covariance function (14) is completely analogous to that of a dampened mechanical oscillator with two different oscillating modes. The two damping constants, τ_1 and τ_2 are related to the distance the disturbance would travel before viscosity dampens it. Finally, it should be noted that oscillating modes are not unlikely in pipe flow, provided the length/diameter ratio of the pipe is greater than 60 (this ratio is 120 in our experiment) [2].

4.2.2 Re = 5 000, X/d = 100

For Re = 5 000, the turbulence begins to grow while the flow progresses downwards. Figure 6 compares the two covariance functions for $X/d = 60$ and 100, respectively. It is possible to see that they are almost indistinguishable each from other, which leads us to conclude that the flow tends to become spatially homogeneous.

Because of the relatively low Reynolds number, we expect the viscous effect to be dominant so that no inertial range has to be expected. For this reason an exponential cut-off in the energy spectrum is expected and, consequently, the covariance function should be well represented by a Lorentzian model,

$$R(\tau) = \frac{1}{1 + (\frac{\tau}{\tau_o})^\alpha} \quad (19)$$

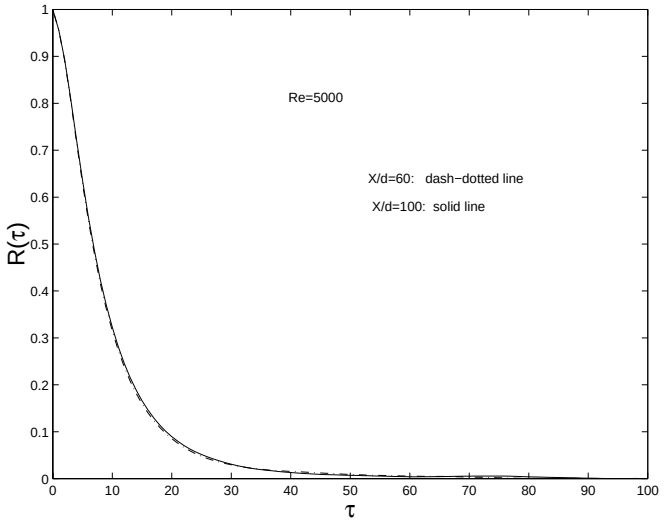

Fig. 6. Comparison between the two normalized covariance functions for $X/d = 60$ (dash-dotted line) and $X/d = 100$ (solid line). The Reynolds number is $\mathrm{Re} = 5\,000$.

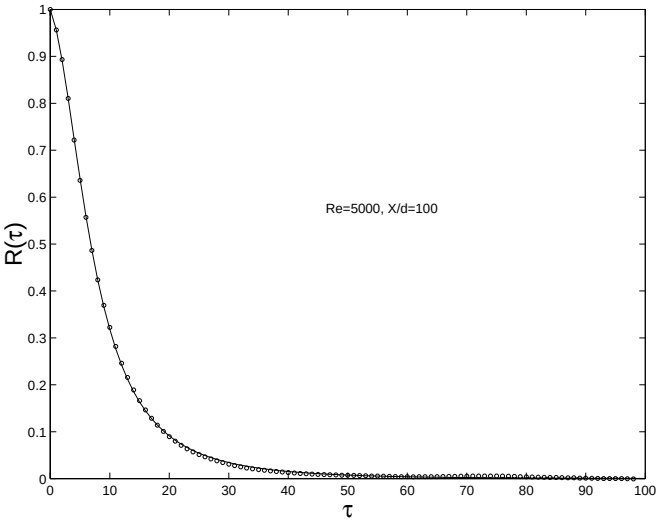

Fig. 7. Covariance function (circles) normalized to the variance of the series, $R(\tau) = C_\mathrm{s}(\tau)/C_\mathrm{s}(0)$, against the normalized time scale, τ. The Reynolds number is $5\,000$, $X/d = 100$. The solid line is the model fitted to the data points.

with the parameter $\alpha = 2$. For τ small enough, the relation (19) predicts that the second-order structure function, $S(\tau) = 2C_\mathrm{s}(0)(1 - R(\tau)) \sim \tau^2$, which is the usual law assumed for the dissipative range.

The model (19) represents very well the correlation structure of the flow. However, it predicts a decaying to zero of $C_\mathrm{s}(\tau)$ which is slightly lower than that observed. Better agreement is found if we allow for an extra exponential damping factor,

$$R(\tau) = \frac{1}{1 + (\frac{\tau}{\tau_\mathrm{o}})^\alpha} \exp(-\frac{\tau}{\mu_\mathrm{o}}). \tag{20}$$

Figure 7 compares the covariance function to the model (20), for $X/d = 100$. Here, α has been considered as an adjustable parameter. We found $\alpha = 1.936 \pm 0.004$ which is very close to the expected value of 2. Indeed, no appreciable difference may bee seen in the model fitted to the data if we just set $\alpha = 2$. For the two cut-off scales, τ_o and μ_o the value of 8.53 ± 0.08 and 35.02 ± 0.05 have been found, respectively. These values may be compared to those obtained for $X/d = 60$: $\alpha = 1.938 \pm 0.004$ $\tau_\mathrm{o} = 8.30 \pm 0.08$ and $\mu_\mathrm{o} = 35.60 \pm 0.05$.

It is quite remarkable that the presence of the second time scale is of the order of the diameter of the pipe. By invoking Taylor's frozen turbulence hypothesis [19], μ_o corresponds to 35.6 mm which may be compared to the diameter of the pipe which is 50 mm. On the other hand, τ_o may be understood as the microscale of turbulence or the typical size of the smallest eddies in the flow [19]. This connection may be made rigorous from a mathematical point of view. According to Tennekes and Lumley [20] the Taylor microscale is associated with the curvature, λ^2 of the autocorrelation function, which in turn is defined by:

$$\frac{\mathrm{d}^2 R(\tau)}{\mathrm{d}\tau^2} \|_{\tau=0} \equiv \frac{-2}{\lambda^2} \tag{21}$$

Taking the second derivative of equation (20) and computing it at $\tau = 0$, we have

$$\frac{\mathrm{d}^2 R(\tau)}{\mathrm{d}\tau^2} \|_{\tau=0} = \frac{-2}{\tau_\mathrm{o}^2} + \frac{1}{\mu_\mathrm{o}^2} \approx \frac{-2}{\tau_\mathrm{o}^2} \tag{22}$$

from which $\tau_\mathrm{o} \approx \lambda$ (we have used $\alpha = 2$). It should be stressed, however, that the Taylor microscale is not the smallest length scale occurring in turbulence [20]). For our experiment, it simply measures the average size of the turbulent patches, which tend to be highly localized. However, the patches themselves still contain eddies.

Finally, it is noteworthy that the large scale exponential damping factor introduces a Lorentzian behavior in the energy spectrum at low values of the wavenumber. This behavior is in agreement with experimental studies on spectral distribution of the longitudinal turbulence velocity component (*e.g.* [19], p. 67, Figs. 1-18 and related discussion in the text) which systematically show a Lorentzian behavior in the part of the spectrum which pertains to low values of frequency/wavenumber.

Finally, we want to stress that the covariance function for $\mathrm{Re} = 5\,000$ and any X/d is badly represented by the linear model (12) for any choice of p. We have also checked that a pure damped (exponential) model ($\beta_i = 0$) yields a poor model for the covariance function. In other words there is no good linear representation for the correlation structure for $\mathrm{Re} = 5\,000$. The disturbances originated in the inlet region of the pipe just progress almost undisturbed downstream and conserves their non-autoregressive correlation structure.

4.2.3 $\mathrm{Re} = 2\,500$, $\mathrm{X/d} = 100$

Figure 8 shows a plot of the covariance function for $\mathrm{Re} = 2500$ and $X/d = 100$. Its long tail is quite evident, however

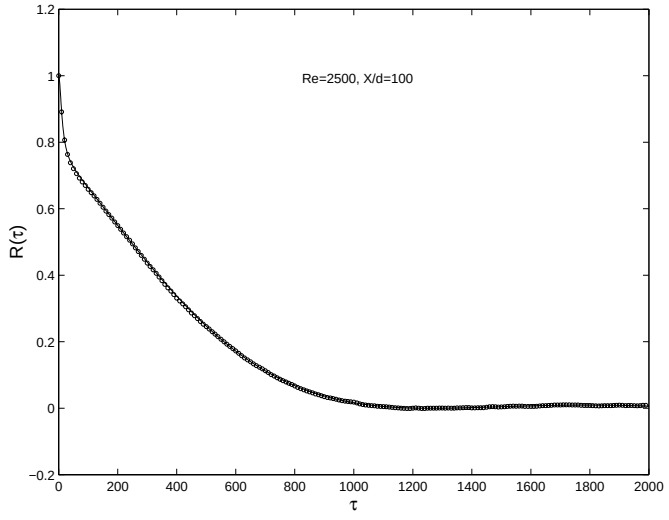

Fig. 8. Covariance function (circles) normalized to the variance of the series, $R(\tau) = C_{\rm s}(\tau)/C_{\rm s}(0)$, against the normalized time scale, τ. The Reynolds number is 2500, $X/d = 100$. The solid line is the model fitted to the data points.

close to the origin the function has an evident cross-over behavior.

We think that the covariance function crosses-over from an algebraic behavior, which characterizes the locally disordered flow (turbulent patches), to a dampened oscillation which is characteristic of the decaying turbulence. In other words, the flow contains both locally disordered flow whose statistical structure is the same as that which characterizes the flow for Re = 5 000 and decaying turbulence which has a behavior as that found, *e.g.*, for Re = 1 500.

To check this hypothesis, we consider for the covariance function the model:

$$\frac{C_{\rm s}(\tau)}{C_{\rm s}(0)} = \sum_{i=1}^{2} a_i \cos(2\pi\frac{\tau}{T_i}) \exp(-\frac{\tau}{\tau_i}) + a_3 \frac{1}{1+(\tau/\tau_{\rm o})^2} \exp(-\frac{\tau}{\mu_{\rm o}}) \qquad (23)$$

with $a_1 + a_2 + a_3 = 1$. The model above is just the composition of a small-scale Lorentzian-exponential decay and a large-scale autoregressive behavior.

The best fit is shown in Figure 8 and we see that the agreement is perfect. The value of the parameters is here summarized:

$$\begin{cases} a_1 = 0.29 \pm 0.02 & a_2 = 0.47 \pm 0.02 \\ T_1 = 776 \pm 25 & T_2 = 2400 \pm 37 \\ \tau_1 = 1450 \pm 190 & \tau_2 = 636 \pm 4 \\ \tau_{\rm o} = 16.0 \pm 0.5 & \mu_{\rm o} = 51.0 \pm 0.5 \end{cases} \qquad (24)$$

and $a_3 = 1 - a_1 - a_2 = 0.24 \pm 0.03$.

This last result just emphasizes that the correlation structure of the turbulent bursts is not autoregressive, so that temporal intermittency by no way can be explained as a spatially localized increase of the level of the linear fluctuations.

To summarize, we have that far away from the inlet, the covariance function obeys the following laws as a function of the Reynolds number:

$$\frac{C_{\rm s}(\tau)}{C_{\rm s}(0)} = \begin{cases} \sum_{i=1}^{2} a_i \cos(2\pi\frac{\tau}{T_i}) \exp(-\frac{\tau}{\tau_i}). & (25.1) \\ (\sum_{i=1}^{2} a_i \cos(2\pi\frac{\tau}{T_i}) \exp(-\frac{\tau}{\tau_i})) \\ +a_3 \frac{1}{1+(\frac{\tau}{\tau_{\rm o}})^2} \exp(-\frac{\tau}{\mu_{\rm o}}). & (25.2) \\ \frac{1}{1+(\frac{\tau}{\tau_{\rm o}})^2} \exp(-\frac{\tau}{\mu_{\rm o}}). & (25.3) \end{cases}$$

where the first of the equations (25) applies to Re = 1 500, the second to Re = 2 500 and the last to Re = 5 000. For Re = 1 500, the character of the fluctuations is linear and mimics $1/f^2$ noise at high frequency. Conversely, for Re = 5 000 the character is Lorentzian-exponential like. At the transition (Re = 2 500) both behaviors are present.

5 Summary and conclusions

In this paper we have analyzed the Reynolds number dependence of the covariance function for pipe flow. Observations of the stream wise component of the velocity field have been reported for different locations along the axis of the tube, namely X/d =20, 60, 100, where X denotes the distance from the inlet and d is the inner diameter of the pipe. The Reynolds numbers we have analyzed cover the range 1 500 to 5 000, that is, transition to turbulence and moderately developed turbulence. The main features of our experimental results can be summarized as follows:

- Turbulence was induced by using a sharp inlet.
- For Re $\leq$ 1800, turbulence did not grow, it was dampened by viscosity and the most interesting characteristics was a very long-range dynamical correlation which yielded $1/f^2$ noise, although as a limiting case of an autoregressive (linear) behavior.
- A cross-over character of the flow was evident in between Re = 2 000−4 000. In this case the most disordered part of the flow was spatially localized in the pipe which yielded the characteristic phenomenon of temporal intermittency. Both decaying and non-decaying turbulence was easily recognized in the flow.
- For values of Reynolds number greater than Re = 4 000 (we have extensively analyzed the case Re = 5 000) the turbulence grew while the flow progressed downstream and tended rapidly towards homogeneity. The covariance function was, then, well described by a Lorentzian-like (algebraic) model with an extra exponential dampening factor.

The correlation structure of developed turbulence was, then, identical to that of the strong bursts present at the onset and was in any case non-autoregressive which leads us to conclude for the presence of a non-linear dynamics.

From a dynamical point of view our results may be interpreted on the basis of a set of differential equation governing the flow. Away from the inlet, the flow is linear below a critical Re and non-linear above. However, our findings are consistent with this picture only if assume that the system is driven by a stochastic force which simulate the disturbances originated at the inlet. Since, these disturbances themselves generate the phenomenon of intermittency, the phenomenon appear to be intrinsically stochastic.

In this respect, our findings seem to be in better agreement with the idea of phase-transition from linear fractality to homogeneity, recently introduced by Bershadskii [21] in a different context. The flow, then, should crosses-over from a random mono-fractal structure to a multifractal structure. Before transition the mono-fractal structure is, indeed, consistent with the $1/f^2$ noise behavior we have evidenced for $\mathrm{Re} = 1\,500$. From our preliminary results on the transition, a multifractal behavior has been evidenced for $\mathrm{Re} = 6\,000$ [22].

References

1. A.G. Darbyshire, T. Mullin, J. Fluid. Mech. **289**, 83 (1995).
2. D.J. Tritton, *Physical Fluid Dynamics* (Oxford Science Publishing, Oxford, 1988).
3. I.J. Wygnanski, F. H. Champagne, J. Fluid. Mech. **59**, 281 (1973).
4. I.J. Wygnanski, F.H. Champagne, J. Fluid. Mech. **69**, 283 (1975).
5. R.H. Kraichnan, D. Montgomery, Rep. Prog. Phys. **43**, 547 (1980).
6. G. Paladin, A. Vulpiani, Phys. Rep. **156**, 147 (1987).
7. A. Libchaber, in *Turbulence and Predictability in Geophysical Fluid Dynamics and Climate Dynamics*, edited by M. Ghil, R. Benzi, G. Parisi (North-Holland, Amsterdam, 1985), p. 17.
8. D. Ruelle, in *Turbulence and Predictability in Geophysical Fluid Dynamics and Climate Dynamics*, edited by M. Ghil, R. Benzi, G. Parisi (North-Holland, Amsterdam, 1985), p. 3.
9. P. Manneville, Y. Pomeau, Commun. Math. Phys. **74**, 189 (1980).
10. F. Durst, A. Melling, J.H. Whitelaw, *Principles and Practice of Laser-Doppler Anemometry*, (Academic Press, London, 1981).
11. G.E.P. Box, G.M. Jenkins, *Time Series Analysis* (Holden-Day, S. Francisco, 1976)
12. K.R. Sreenivasan, R. Ramshankar, Physica D **23**, 246 (1986).
13. J. Zhang, D. Stassinopoulos, P. Alstrom, M.T. Levinsen, Phys. Fluids **6**, 1722 (1994).
14. D. Ruelle, *Chaotic evolution and strange attractor* (Cambridge University Press, Cambridge, 1988).
15. A.D. Nychka, S. Ellner, R. Gallant, D. McCaffrey, J. R. Stat. Soc. B **54**, 399 (1992).
16. J.D. Farmer, J.J. Sidorowich, Phys. Rev. Lett. **59**, 845 (1987).
17. C. Serio, Il Nuovo Cimento B **6**, 681 (1992).
18. C. Serio, Europhys. Lett. **27**, 103 (1994).
19. J.O. Hinze, *Turbulence* (McGraw-Hill, New York, 1975).
20. H. Tennekes, J.L. Lumley, *A First Course in Turbulence* (The MIT Press, Cambridge, 1994).
21. A. Bershadskii, Phys. Lett. A **222**, 375 (1996).
22. R.M. Di Tommaso, F. Esposito, R. Laurenzana, E. Nino, C. Serio, Europhys. Lett. **36**, 669 (1996).